Cavitation bubble collapse and wall shear stress generated in a narrow gap

[1]Silvestre Roberto Gonzalez-Avila; [2]Anne Charlotte van Blokland; [1]Qingyun Zeng; [1,3]Claus-Dieter Ohl

[1]*Nanyang Technological University, Singapore; [2]University of Oxford, United Kingdom;*
[3]*Otto-von-Guericke University of Magdeburg, Germany.*

Abstract

Cavitation bubble dynamics in narrow gaps confined by rigid boundaries greatly differs from a liquid half-space. There exists a regime, where the bubble is created on one side of the gap and collapses on the opposite side [1]. Additionally, the jet velocities may be considerably larger. The oscillating bubble and the impacting jets form complex boundary layer flows with greatly increased wall shear stress. The observations have implications for cleaning applications in narrow spaces. The experimental results show that the shear flow generated is active much longer after the collapse of the bubble. The results show approximately a 3-fold increase of the shear stress as compared to a liquid half space. We also present a space-time graph from numerical simulations. Additionally, the fluid dynamics is studied with the motion of particles attached to a substrate and the effect of shear on adherent biological cells.

Keywords: Wall shear stress; bubble dynamics; particle removal

Introduction

Cavitation near boundaries generates large forces on boundaries through normal and tangentially acting stresses. Viscosity is responsible to transmit tangential surface forces, which are particularly important for cleaning and biological cell applications. After studying the flow in greater detail [2, 3] we became interested on the flow occurring between two parallel plates separated by a thin gap [1]. We revealed that cavitation bubbles created might migrate from the location where they are created to the opposite plate. Thus the aforementioned forces occur at some distance from the bubble creation. This could lead to applications of cleaning in thin gaps such as in stacks of membranes for water treatment or to induce forces on cells while preventing a physical contact of the bubble generator to the cells.

Besides the translational movement we have seen considerably higher velocities of the jet using inviscid boundary element simulations. This suggests that the wall shear stresses could also be higher in a thin gap as compared to a similar sized bubble in a semi-infinite liquid. To test this hypothesis we measure the wall shear stress and additionally conduct viscous computational fluid mechanics simulations.

Then we present results on cleaning and cell removal/drug delivery to show the advantages of the geometry. All bubbles presented here are created with a spark discharge using a simple high-voltage sparker.

Bubble Dynamics

The experimental setup consists of a piezoelectric igniter connected to two electrodes where the cavitation bubbles are created, an oscilloscope (LeCroy HRO 64zi, 2 GHz maximum sampling rate), and a high-speed camera (Photron SAX2). The electrodes on a printed circuit board (PCB) are made of copper by an etching method as described by [4]; the thickness of the wires is ~125 μm and the separation between them is ~ 150 μm although these dimensions vary ~ ±20 μm due to the etching process. The piezoelectric igniter starts the events; it creates a spark between the electrodes, which creates a hemispherical cavitation bubble originating from the PCB. To measures the wall shear stress a hot film anemometer 55R46 (Dantec Dynamics, 10 kHz bandwidth) is flush mounted in the boundaries, see figure 1a. The hot film anemometer and the electrodes were submerged in a cubic container of 75 mm in side and mounted on a 3-axis stage; in this way the relative position of the electrodes and the wall shear stress sensor can be adjusted accurately. The rising signal detected by the anemometer starts the data acquisition process, the oscilloscope triggers then the high-speed camera. The relevant experimental parameters are depicted in figure 1b; H is the distance between the walls, R_x the maximum radius attained by the bubble in the horizontal direction and δ is the horizontal distance between the center of the bubble and the hot film sensor.
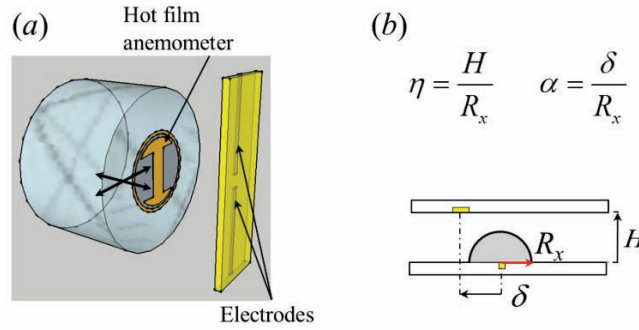
Figure 1. (a) Schematic diagram of the experimental setup (b) experimental parameters

The experiments are complimented with a compressible volume of fluid simulation using OpenFOAM. The simulation domain is axisymmetric (radial size is 5 mm, height 0.75 mm). An initial grid with 100x15 cells is refined recursively five times leading to a cell size of about 1.5 μm where the bubble is located. The simulation omits the nucleation dynamics and starts with an initially spherical gas bubble located at a distance of 250 μm above the wall with a radius of 50 μm and initial pressure of $p_g(t = 0) = 1250$ bar. The solver accounts for surface tension and liquid viscosity. A detailed discussion of the techniques and limits is provided in [5].
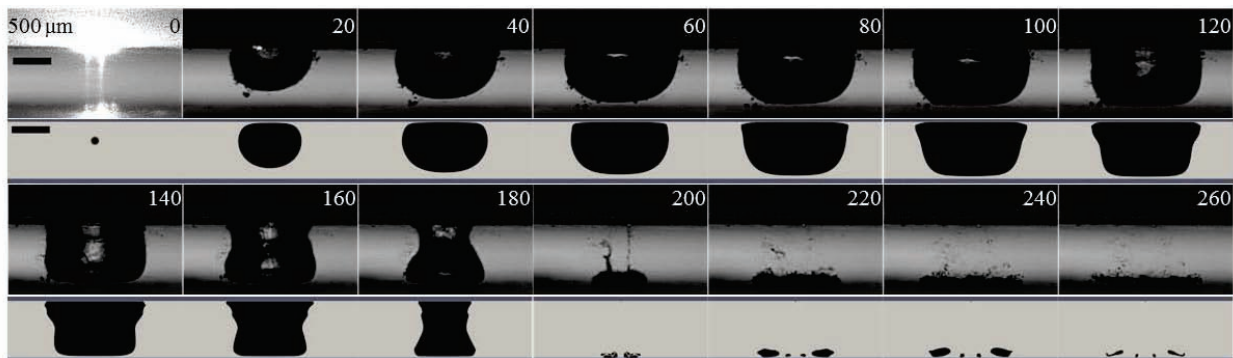

Figure 2. Comparison of experiment and simulation for a bubble of R_x = 770 μm and h = 750 μm. The upper row is the high-speed images, the lower row is the simulation result. The upper boundary is the nucleated wall and the lower boundary is the opposite wall. Time is in μs.

Figure 2 presents a bubble nucleated in a regime where the migration to the opposite wall takes place. The figure also depicts a comparison between experiment and a simulated bubble dynamics for R_x = 770 μm and h = 750 μm. The interval between frames is 20 μs for both sequences. At t = 0 the simulated bubble expands from a small spherical volume while the bubble in the experiment is nucleated on the surface. Despite the simplifications introduced in the simulations a rather good agreement of the bubble shape is obtained already after t = 20 μs. The bubbles in the experiment and the simulation reach their maximum size at $t \sim$ 100 μs with a cap shape. During the early stage of the collapse, the middle part of the bubble collapses faster than the other parts and an hourglass shape bubble is formed. However, after t = 160 μs the part closer to the wall where the bubble is nucleated shrinks faster and a jet is formed directed to the opposite wall. The jet penetrates the bubble wall and impacts on the opposite surface creating a strong radial shear flow. The toroidal bubble reaches its minimum size at around t = 200 μs and rebounds to a much smaller maximum size than that in the first cycle at around t = 240 μs. The overall bubble dynamics is nicely reproduced by the simulations. We therefore discuss the simulated wall shear stress first before we look into the measured data.

Wall Shear Stress
The wall shear stress is defined as

$$\tau = \mu \frac{du_r}{dy}\bigg|_{y=0} \tag{1}$$

where μ is the liquid's viscosity, u_r the flow velocity component parallel to the wall and y is the distance to the boundary. Figure 3 presents the spatio-temporal wall shear stress map on both walls for a bubble of $R_x = 770$ μm and $h = 750$ μm. We take a logarithm base 10 of the shear stress value due to its large range. The stress directed away from the axis of symmetry is colored in red, while the negative values in blue color represents the stress towards the axis of symmetry. The high stresses occur approximately when the bubble reaches its minimum size at $t \sim 200$ μs on both walls , about $20 \sim$ kPa on the nucleated wall and $100 \sim$ kPa on the opposite wall. The stress is positive in the whole domain during most of the expansion, $0 \leq t \leq 50$ μs, on both walls due to the rapid expansion of the bubble. At the later stage of the expansion and the early period of the following shrinkage, the stress is still positive within the domain between the bubble wall and the boundary and becomes negative outside the bubble domain because of the incoming flow, due to the deformation and collapsing of the bubble. Note that for the above period, the positive stress decreases with time while the negative increases with time, and a large area with almost zero stress occurs on the nucleated wall before the formation of the jet. High stresses are found at $t \sim 195$ μs near the axis of symmetry ($r = 0$), which come from the impact and spread of the liquid jet which penetrates through the bubble.

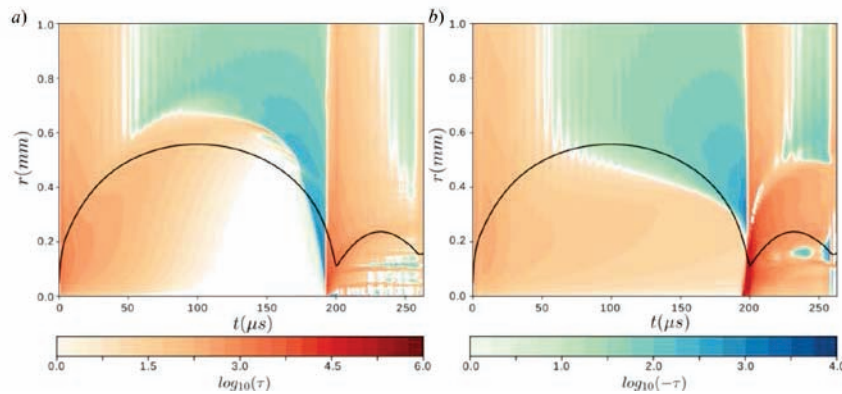Figure 3. Wall shear stress for $R_x = 770$ μm, $h = 750$ μm. (a) on the wall the bubble is nucleated; (b) on the opposite wall. The black curve is the bubble equivalent radius. The wall shear stress is in Pa; positive values represent flow along the positive radial direction, negative towards the axis of symmetry.
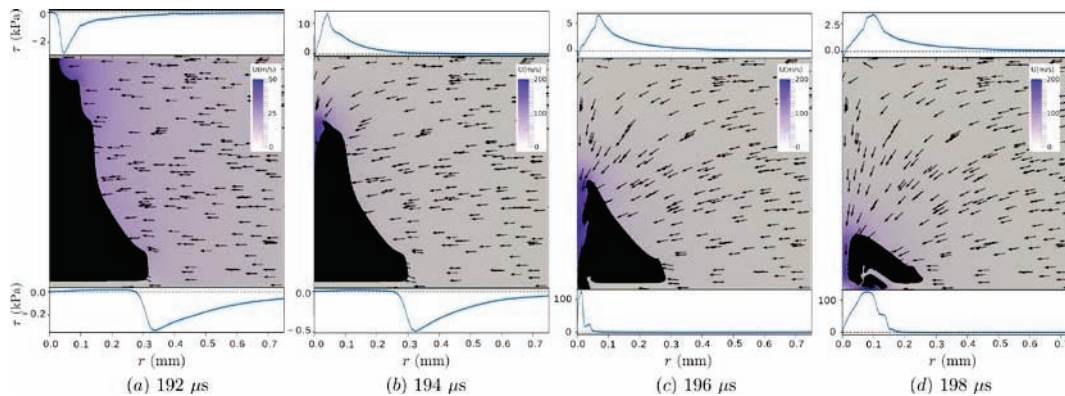

Figure 4. The jet formation and wall shear stress distribution on the upper and lower walls for a bubble of $R_x = 770$ μm, $h = 750$ μm. The bubble is nucleated on the top wall. The black region is the bubble. The plots above and below the flow fields are the wall shear stress distribution along the radial directions on each wall. The arrows show the direction of the liquid flow. Negative wall shear stress values represent flow towards the axis of symmetry while positive values represent flow in the positive radial direction.

Figure 4 portrays this jet formation process, as well as the wall shear stress distribution on both walls. Before the jet is formed, the stresses are negative in the regime outside the bubble and the negative peaks are located near the outside boundary of the hourglass shape bubble with a lowest value of about -2.5 kPa on the nucleated wall and -0.5 kPa on the opposite wall. When the jet starts to be formed a high positive stress of 12 kPa appears on the nucleated wall ($t = 194$ μs), which is due to the impact and spread of the recoiled flow of the initial jet. However, this recoiled

flow is much weaker than the jet-induced flow thus the shear stress is damped quickly, see figure 4b-d. The jet accelerates due to the collapsing bubble and reaches approximate 200 m/s when it impacts the lower bubble wall.

We now discuss the experimentally recorded wall shear stress, shown in figure 5a. Each curve in the figure depicts the wall shear stress for a different distances from the bubble, α. In these tests the channel height, H, is kept fixed, as shown in the inset of figure 5b, and the wall shear stress, τ, is evaluated when the offset parameter is varied in the range $0.1 \leq \alpha \leq 2.1$; three curves of increasing δ/R_x values are shown. The width of the shaded boxes represents the collapse time of the cavitation bubble, from maximum expansion to its minimum volume; the height of each box represents the increase in shear stress during the bubble's collapse time. At $\delta/R_x = 0.1$ the τ vs t exhibits a maximum value at $t = 261$ µs and a second maximum at $t = 701$ µs; the first maximum is produced by the re-expansion of the cavitation bubble; we believe the second maximum may be due to the vortex generated after the bubble's collapse. This curve also displays a third and small peak at $t = 3.1$ ms but we cannot tell from the video why the curve is distorted. The maximum τ value seen in the curves of $\delta/R_x = 0.8$ and $\delta/R_x = 1.9$, at $t = 381$ µs and at $t = 1.2$ ms, respectively occur much later after the bubble's collapse, thus this peak is more like due to the vortex generated; also note that the peak of the curve of $\delta/R_x = 1.9$ is ~ 1% of that of the curve of $\delta/R_x = 0.1$. Figure 5b portrays the summary of the peak τ value recorded at the different α values tested. The maximum τ values recorded decrease very rapidly, thus the maximum stress generated 2 radii away is ~ 1% of the value at recorded at $\delta/R_x = 0.1$. This is in agreement with previous studies that show that the effect of cavitation bubbles is very localized [3,4,6].
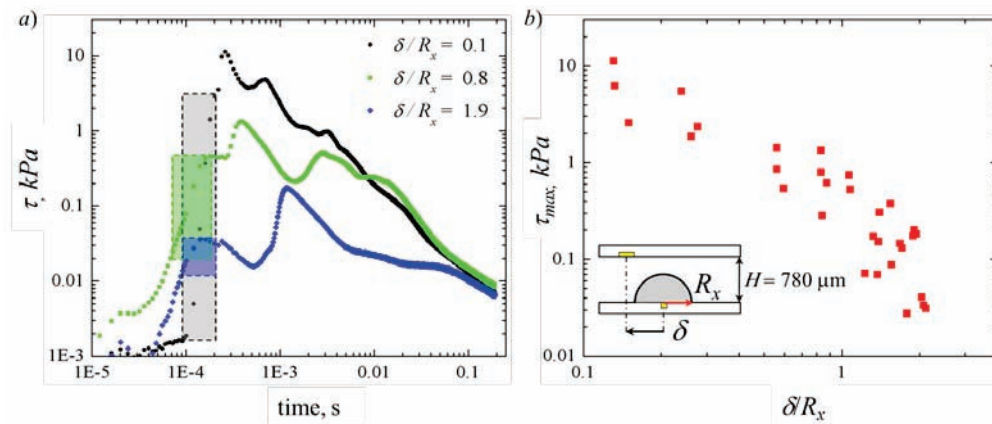

Figure 5. (a) Wall shear stress vs time for different lateral positions; (b) τ_{max} vs δ/R_x; H is kept constant. $R_x = 730 \pm 50$ µm (average of 33 tests).

Experimental and numerical results

As was shown in figure 2 the overall bubble dynamics is well reproduced by the simulations. However, there is a significant difference in the measured and simulated peak shear stress values. We believe that the peak shear stress detected is underestimated due to the low bandwidth of the anemometer, yet our results show that the peak measured shear stress value is ~ 3 times larger than that previously reported for a bubble of similar size created next to a single boundary [3]. The simulations are especially useful to interpret the complex flow generated at the bubble collapse (i.e., see figure 4a-d) which is too fast to be resolved even by the high-speed camera. In addition to that, the wall shear stress distribution in space and as a function of time is available from the simulations, a large number of experiments would be needed to create such a map due to the point wise nature of the hot film probe. In the next subsections, we indicate two potential applications where this shear flow can be utilized: cleaning in a narrow gap and drug delivery into adherent cells.

Cleaning in a narrow gap

Fluorescent polystyrene particles with a diameter of 15 µm are prepared by letting droplets with suspended particles evaporate on a heated glass substrate. This leads to a characteristic distribution of weakly bonded particles on an

annular ring, see first frame in figure 6, which remains even after the substrate is re-suspended in water. In the cleaning experiments, the substrate with the attached particles forms the lower boundary in the gap. The bubble is created on the upper plate by activating the high voltage source. Figure 6 depicts the motion of the fluorescent particles exposed to a bubble following a very similar dynamics as in figure 2 (η =1.0). The six frames in figure 6 depict the particles before (t = -28 μs), during ($0 \leq t \leq 222$ μs) and after (t = 138 ms) the cavitation event. The bubble is created from a spark discharge visible in figure 6 (t = 0) with a bright region at the center. A first motion of the particles is visible during the expansion phase t = 56 μs where they are dragged outwards. During the bubble shrinkage the inward flow drags the particles towards the center, see arrows at t = 195 μs. Interestingly while the expansion of the bubble accelerates the particles purely radially there is a circumferential instability of the inward flow visible at time t = 195 μs. Once the bubble collapses a fast jet is created which reverses the particle motion as indicated with the arrows at t = 222 μs. This back and forth motion leads to complex boundary layer flow dispersing the particles such that the initial annular ring shape is lost, see figure 6 at t = 138 ms. Also, the particles have been removed from the field of view either by moving out of focus or being transported out of the observation area through the residual flow generated by the bubble.
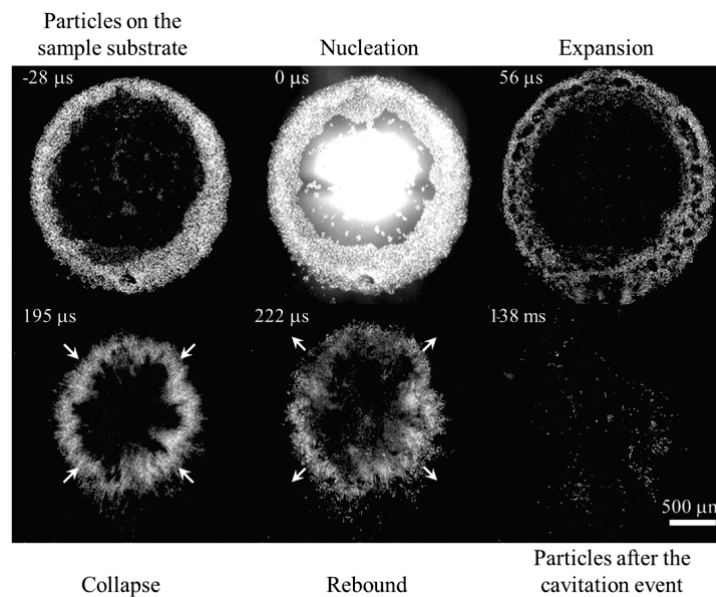

Figure 6. Fluorescent polystyrene particles removed by a spark-generated cavitation bubble, η = 1.0.

Molecule transport into cells

It is known that biological cells with a plasma membrane can be temporarily opened for the transport of large molecules through shear stress. The flow responsible for the particle motion in figure 6 demonstrates that although the cavitation is created as some distance from the substrate strong shearing flow can be create. We explore if it is feasible to induce pores in cell membranes. This geometry has the advantage that the cells do not need to be in contact with the device creating the flow. Additionally, the strength of the flow may be adjusted by changing the height of the gap H as shown in figure 7a.
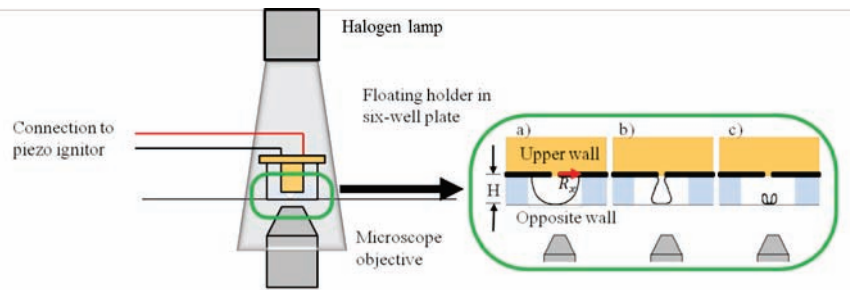
Figure 7. Sketch of the device and experimental setup to study drug delivery into cells. The electrodes are on a separate device, which is placed onto a petri-dish with the adherent cells. The cells and bubble dynamics is recorded from below though an inverted microscope.

For the experiments we use colon carcinoma cells (RKO). An added complexity is the electrical discharge to generate the bubbles. As the cell medium is conductive we add a thin layer of low viscosity silicon oil (5cSt) on top of the cell medium. The microscope objective is focused on the substrate with the cells, thus the bubble initially growing on the upper wall with electrodes is out of focus, see figure 8a, $t = 3.7$ μs. After bubble expansion it collapses onto the opposite wall at $t = 119$ μs with a torus shape due to the jet that pierces through it. The size of this jet area is comparable to the size where molecular uptake is taking place, see figure 8b.
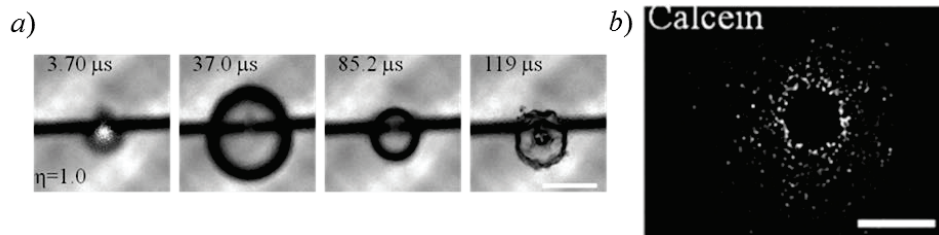

Figure 8. Fluorescent uptake of Calcein in the RKO cells for $\eta = 1.0 \pm 0.1$. (a) high-speed images of the bubble dynamics; (b) fluorescent image of cells taken up the non-membrane permeant dye Calcein. The scale bar is 500 μm.

Conclusion

Bubble collapse between two walls can produce wall shear stresses of up to 10kPa near the site where the bubble collapses; this is likely a lower bound of the shear stress reached due to the low bandwidth of the hot film probe of 10kHz. Nevertheless, the maximum shear stress measured is ~ 3 times larger than the values found in bubbles of similar size collapsing near a single wall [3]. The flow generated by the cavitation bubbles remains long after the cavitation event ends. However, a large number of tests are required to obtain a shear stress distribution on a solid wall. Due to this, numerical simulations are presented. A space-time diagram depicts the shear stress attained by a single cavitation event for specific η value. Also, we have shown that a very simple device, with no moving walls can be used to generate such a high shear flow; in addition to that, two potential applications are demonstrated, the removal of particles attached to a substrate and molecule transport though the cell membrane. The flow generated by a migrating bubble can also be used to produce fast microjets; this topic has received significant attention recently [7,8,9] due to their potential to deliver drug without needles.

References

[1] Gonzalez-Avila, S.R., Klaseboer, E., Khoo, B.C., Ohl, C.D. (2011). *Cavitation bubble dynamics in a liquid gap of variable height*. J. Fluid Mech., 682.

[2] Ohl, C-D., Arora, M., Dikink, R., de Jong, N., Versluis, M., Delius, M., Lohse, D. (2006). *Sonoporation from Jetting Cavitation Bubbles*. Biophysi J. 91, 4285–429.

[3] Dijkink, R., Ohl, C-D. (2008). *Measurement of cavitation induced wall shear stress*. Appl Phys Lett, 93, 254107.

[4] Gonzalez-Avila, S. R., Huang X., Quinto-Su, P. A., Wu, T., Ohl, C-D. (2011). *Motion of micrometer sized spherical particles exposed to a transient radial flow: attraction, repulsion, and rotation*. Phys Rev Lett, 107, 074503.

[5] Zeng, Q., Gonzalez Avila, S-R., Dijkink, R., Gavaises, M., Ohl C-D (2017). *Wall shear stress from setting cavitation bubbles*. Submitted to the J. Fluid Mech.

[6] Kim, W., Kim, T. H., Choi, J., Kim, H. Y. (2009). *Mechanism of particle removal by megasonic waves*. Appl. Phys. Lett. 94, 081908.

[7] Karri, B., Gonzalez-A., S. R., Loke, Y. C., O'Shea, S. J., Klaseboer, E., Khoo, B. C., Ohl, C-D. (2012). *High-speed jetting and spray formation from bubble collapse*. Phys. Rev. E 85, 015303.

[8] Tagawa, Y., Oudalov, N., El Ghalbzouri, A., Sun, C., Lohse, D. (2013). *Needle-free injection into skin and soft matter with highly focused microjets*. Lab Chip 13, 1357–1363.

[9] Gonzalez-Avila, S. R., Song, C., Ohl, C-D. (2015). *Fast transient microjets induced by hemispherical cavitation bubbles*. J. Fluid Mech., 767, 31-51.

© 2018 ASME